Journal of Molecular and Cellular Cardiology 106 (2017) 68–83

Contents lists available at ScienceDirect

Journal of Molecular and Cellular Cardiology

journal homepage: www.elsevier.com/locate/yjmcc

A model of cardiac contraction based on novel measurements of tension development in human cardiomyocytes

Sander Land[a,*], So-Jin Park-Holohan[b], Nicolas P. Smith[c], Cristobal G. dos Remedios[d], Jonathan C. Kentish[b], Steven A. Niederer[a]

[a] Department of Biomedical Engineering, King's College London, UK
[b] Cardiovascular Division, King's College London British Heart Foundation Centre of Research Excellence, UK
[c] Department of Engineering Science, University of Auckland, New Zealand
[d] Department of Anatomy and Histology, University of Sydney, Australia

ARTICLE INFO

Article history:
Received 14 October 2016
Received in revised form 12 January 2017
Accepted 31 March 2017
Available online 7 April 2017

Keywords:
Cardiac muscle
Force generation
Viscoelasticity
Human cardiomyocytes
Computational modelling

ABSTRACT

Experimental data from human cardiac myocytes at body temperature is crucial for a quantitative understanding of clinically relevant cardiac function and development of whole-organ computational models. However, such experimental data is currently very limited. Specifically, important measurements to characterize changes in tension development in human cardiomyocytes that occur with perturbations in cell length are not available. To address this deficiency, in this study we present an experimental data set collected from skinned human cardiac myocytes, including the passive and viscoelastic properties of isolated myocytes, the steady-state force calcium relationship at different sarcomere lengths, and changes in tension following a rapid increase or decrease in length, and after constant velocity shortening. This data set is, to our knowledge, the first characterization of length and velocity-dependence of tension generation in human skinned cardiac myocytes at body temperature.

We use this data to develop a computational model of contraction and passive viscoelasticity in human myocytes. Our model includes troponin C kinetics, tropomyosin kinetics, a three-state crossbridge model that accounts for the distortion of crossbridges, and the cellular viscoelastic response. Each component is parametrized using our experimental data collected in human cardiomyocytes at body temperature. Furthermore we are able to confirm that properties of length-dependent activation at 37 °C are similar to other species, with a shift in calcium sensitivity and increase in maximum tension. We revise our model of tension generation in the skinned isolated myocyte to replicate reported tension traces generated in intact muscle during isometric tension, to provide a model of human tension generation for multi-scale simulations. This process requires changes to calcium sensitivity, cooperativity, and crossbridge transition rates. We apply this model within multi-scale simulations of biventricular cardiac function and further refine the parametrization within the whole organ context, based on obtaining a healthy ejection fraction. This process reveals that crossbridge cycling rates differ between skinned myocytes and intact myocytes.

1. Introduction

Computational models of human cardiac function are increasingly used to study cardiac physiology in health and disease [2,3,15,50]. These complex multi-physics and multi-scale cardiac simulations combine models that represent the distinct physiology of the material properties, cellular electrical activity and cellular contraction. When constructing multi-scale models of human function, there are currently many options for characterizing the cellular electrophysiology [19,52] or material properties [48,66]. Detailed biophysical models of cardiac contraction do exist for other species [8,36,56] and have been used to great effect in multi-scale computational models, particularly in the mouse [40,59] and rat [39,51]. These models have the advantage that they can be used to link changes in sub-cellular properties to whole organ contractile performance, predicting key indicators of cardiac function from changes to individual channels or proteins involved in calcium regulation and contractile dynamics. However, there remains a deficit of human biophysical models of tension generation which can be embedded within models of whole organ contraction. Currently whole organ frameworks typically rely on phenomenological models of

* Corresponding author at: Department of Biomedical Engineering, St Thomas' Hospital, London SE1 7EH, UK.
E-mail address: sander.land@kcl.ac.uk (S. Land).

http://dx.doi.org/10.1016/j.yjmcc.2017.03.008
0022-2828/

cellular function [30,58] or models preferentially fitted to animal data [64].

A major reason for this disparity between human and animal models is the historically poor availability of contraction data from human isolated myocytes, trabeculae and muscle strips. Specifically, although data for isometric twitch contractile function exists [44,53] and has been used to parametrize contraction models [36,64], comprehensive data sets for human myocyte contractile function which characterize length- and velocity-dependence of tension generation are not available. In addition, many measurements across species are taken at lower temperatures, including measurements of human myofibrils [54], which limits their application for explaining whole organ contractile function. Finally, the assumption that rapid reactions can be approximated as being in steady-state that can be valid in the faster contractile dynamics of rodent hearts may not be valid in the slower contractile dynamics in humans. This limits the ability to simply re-parametrize a small animal model.

In this study we address these deficits by presenting a comprehensive new data set in human cardiac myocytes at 37 °C, measuring the relation between force, calcium concentration and sarcomere length, the response to fast changes in length, and the passive viscoelastic response of these cells. We then use this data to develop a new model of human cardiac contraction, which is suitable for multi-scale modelling, based on the hypothesis that our preparations in skinned cardiac myocytes have crossbridge dynamics consistent with intact cells in whole organ function, and compare our predictions from skinned myocyte data with literature data from intact myocytes and expected whole organ ejection. Finally, we apply this model to quantify differences between skinned myocytes and cellular function in the heart.

2. Methods

Our experimental data includes measurements of passive elasticity, steady-state force calcium relationships at different sarcomere length, and dynamic changes in tension generation during length perturbations in isolated myocytes. Frozen samples of left ventricular myocardium from healthy unused donor hearts were obtained from the Sydney Heart Bank in Australia. The experimental set up and procedures were generally similar to those reported previously [23], except that the force measurements were made at a solution temperature of 37 °C rather than 15 °C.

2.1. Solutions

Relaxing solution contained (mM) BES 100, K propionate 55, Na_2 phosphocreatine 10, Na_2H_2ATP 6.21 (for $MgATP^{2-} = 5$), $MgCl_2$ 6.24 (for $Mg^{2+} = 1$), dithiothreitol 2, EGTA 10, Pi 1.2, AEBSF 1, leupeptin 0.002 and E64 0.002; pH 7.1 at 37 °C, ionic strength 0.20 mol/L. For pre-activating solution 9.85 mM of the EGTA was replaced by HDTA, while for activating solutions 4–10 mM of the EGTA was replaced by CaEGTA. Maxchelator software (http://maxchelator.stanford.edu/) was used to calculate Ca^{2+} concentrations under the different experimental conditions.

2.2. Cell preparation

Fragments of the samples were thawed and single cardiac myocytes and myocyte fragments were prepared by careful glass homogenization of the tissue. The myocytes were permeabilised with 0.5% Triton X-100 v/v (Sigma Aldrich) in relaxing solution for 30 min at room temperature. The homogenate was centrifuged (4000 rpm, 4.5 min) and the myocyte pellet was washed three times in cold relaxing solution (4 °C) to thoroughly remove any traces of Triton X-100. The myocyte suspension was stored on ice and used within 48 h. The ends of a skinned single myocyte were glued at room temperature using Silicon adhesive (Aqua-Sil, Den Braven) or UV-setting glue (OA63 adhesive and Opticure LED-200 UV light source, Norland), between pins extending from a force transducer and a high-speed length controller (403A and 315C-I, Aurora Scientific Inc., Ontario, Canada).

2.3. Measurements of passive viscoelasticity

Passive viscoelasticity was first measured using a series of five 1s step stretches with the myocyte in relaxing solution [23]. Resting sarcomere length (measured using Aurora HVSL.901A video analysis software at 200 Hz) was set to 1.95–2.05 μm in relaxing solution. Clampex (pClamp, version 10.3, Molecular Devices) was used to record data and control the motor and perfusion systems.

2.4. Measurements of steady-state force-calcium relationship and dynamic response to fast stretches

After measurement of passive viscoelasticity, a fast perfusion system (SF-77B, Warner Instrument Corp) was used to activate each myocyte in the following sequence: pre-activating solution for 4–5 s, activating solution for 7 s, relaxing solution for 5 s (Fig. 1). During steady Ca^{2+} activation the cell was released by 10% of resting cell length (CL), then re-stretched 40 ms later, to help stabilize the sarcomeres. After 1–2 s, when force recovery from the release/restretch was complete, the cell was stretched by 0.5%, 1%, or 2% of CL in 10 ms, and held there for 1s. This stretch was slower than we used previously (2 ms [23]), but was done to minimize cellular damage, as the myocytes appear less robust at 37 °C than at the temperature of 15 °C used previously. After selecting for data quality and noise levels, we have $n = 5$ traces where 0.5% and 2% stretch was applied, and $n = 11$ traces where a 1% stretch was applied, due to more experiments being performed with 1% stretch protocol. The activation protocol was repeated for a range of calcium concentrations. Any decline in isometric force development was measured and corrected for using a reference activating solution (pCa 5.96 or 5.81) applied at intervals. The experiment was terminated when isometric force had declined by more than 20% from the first activation; this usually occurred after about 30 activations. When determining the force-calcium relation for SL = 1.8 μm, 2.0 μm or 2.2 μm, the SL was set with the myocyte in relaxing solution. Since 1.8 μm is below the slack length of the sarcomere (~1.9μm), to set the SL to be 1.8 μm in the activated cell, the relation between SL and cell length was first determined in the relaxed myocyte using a series of length steps over the SL range 1.9 to 2.2 μm, then the cell was shortened to the length that would allow the sarcomeres to shorten during activation to SL = 1.8μm, as estimated from extrapolation of the SL-cell length relation.

2.5. Measurements of dynamic response to constant velocity shortening

Methods for this protocol were identical to those for the dynamic response to fast stretches, except for the change in cell length applied. During steady Ca^{2+} activation the cell was shortened by 7–11% of resting cell length (CL) starting from a sarcomere length of 2.3 μm, with a ramp of duration 100–300 ms, that is, with a velocity of 0.54 to 2.53 μm/s.

3. Results

We develop our multi-scale model of cardiac contraction by sequentially adding model complexity and experimental data, starting with the passive force, then steady-state activation, velocity-dependent dynamics, isometric twitch kinetics, and finally whole-organ contraction.

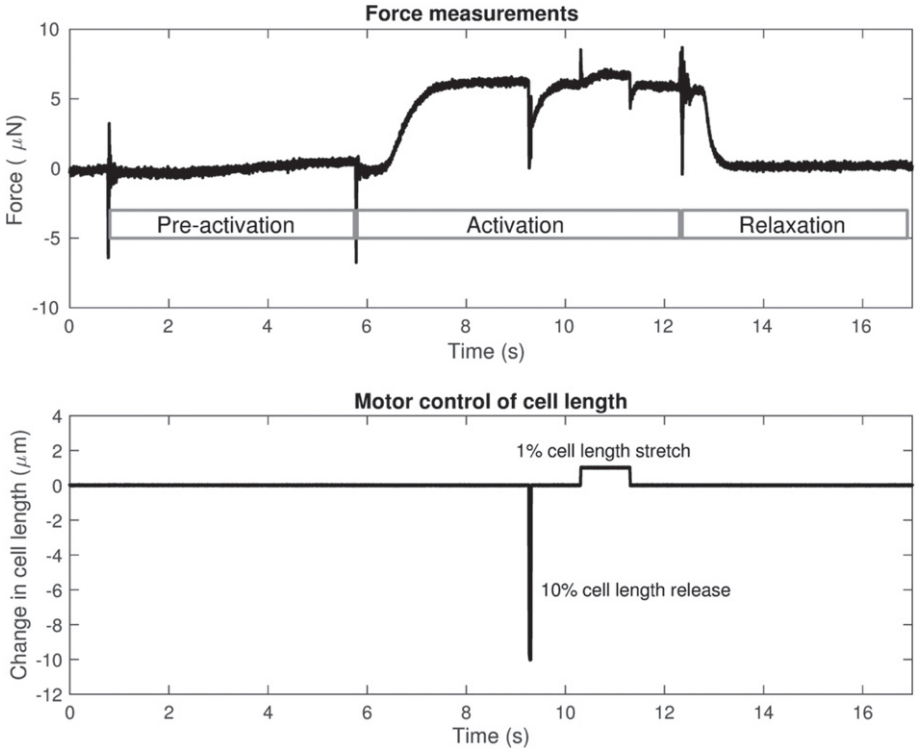

Fig. 1. Experimental protocol and example measurement trace. Force is shown in the top panel, with the change in cell length in the bottom panel. After activation to steady-state force, and a brief release/re-stretch protocol to help stabilize the sarcomeres, dynamic function is measured using a 1% increase and decrease in cell length, before applying a relaxing solution.

Our experimental results and modelling are described in the following sections. Firstly, in Section 3.1 we develop a model of the passive viscoelastic response of the human cardiac myocytes. This model is independent of the fitting of the active tension model in subsequent sections, and is kept constant throughout later modelling. Section 3.2 describes the model of active contraction. In Section 3.3 we fit this active tension model to measurements of the steady-state force-calcium relationship at different sarcomere lengths. Next, in Section 3.4 we extend this model to include the response to dynamic length- and velocity changes, keeping parameters fitted in the steady-state and constraining additional parameters. We adjust the resulting model of a skinned myocyte to represent intact muscle function, by fitting the model to measurements of isometric twitch data from the literature in Section 3.5. Finally, in Section 3.6 we create a multi-scale model of biventricular cardiac mechanics, and use it to further refine our cellular model of an intact myocyte, for optimal use in a whole organ model.

3.1. Passive viscoelastic model

Myocytes, in addition to sharing elastic properties with other types of cells, have a particular viscous response, thought to derive primarily from the molecule titin, which is part of the contractile apparatus [43]. We assume the passive response is independent of other experimental data on active tension presented in this manuscript, due to the presence of a relaxing solution, which suppresses active tension generation to negligible levels.

The data set used to constrain the parameters for the model of passive viscoelasticity includes measurements of sarcomere length, force, and cell area for $n = 7$ cells, and five different step sizes per cell, stretching the cell by 2–10%. Maximal tension development shows high variability, reaching 3.2 ± 1.45 kPa at the end of the decay of the biggest step. We attribute this in part to variability and uncertainty in the cell area as it was measured prior to stretch and not recorded dynamically during experiments. Another potential source of variability is the variable amount of endomysial collagen in these preparations, which may contribute to cell stiffness. To compensate for this variability, experimental data was normalized to have identical force at the end of the last stretch (equal to the mean over all experimental traces).

Fig. 2 shows the mean change in length in the upper panel and the mean and individual normalized force measurement in the lower panel. There is a clear viscous component to the force as indicated by the large spikes and subsequent decay after a quick stretch. This viscous component represents $44 \pm 5\%$ of total passive force, and 75% of this force decays within 92 ± 24 ms. On shortening, the viscous response is significantly smaller, potentially due to a much faster decay rate and recovery during the duration of the shortening step.

The passive response was modelled using a three-parameter model similar to a standard linear solid, consisting of a dashpot and spring in series, in parallel with another spring (see Fig. 2C). This model was chosen for its simplicity and its ability to capture the passive and viscoelastic response shown in our experimental data. To reproduce the typical exponential force-length relationship seen in both our data, and previous experiments in isolated cells and cardiac tissue [23,31,66], the parallel spring F_1 has an exponential behaviour. However, to both limit the number of parameters, as well as ensure an analytical solution to the series force constraint (Eq. (7)), we use a linear relationship for the spring F_2 in series with the dashpot. The dashpot element has separate parameters for shortening and lengthening to accommodate the difference in viscous forces observed.

These considerations result in the following set of equations for our passive tension model:

$$\lambda = \mathrm{SL}/\mathrm{SL}_0 \qquad \text{(extension ratio, as in e.g. [37])} \qquad (1)$$

$$C = \lambda - 1 \qquad \text{(strain)} \qquad (2)$$

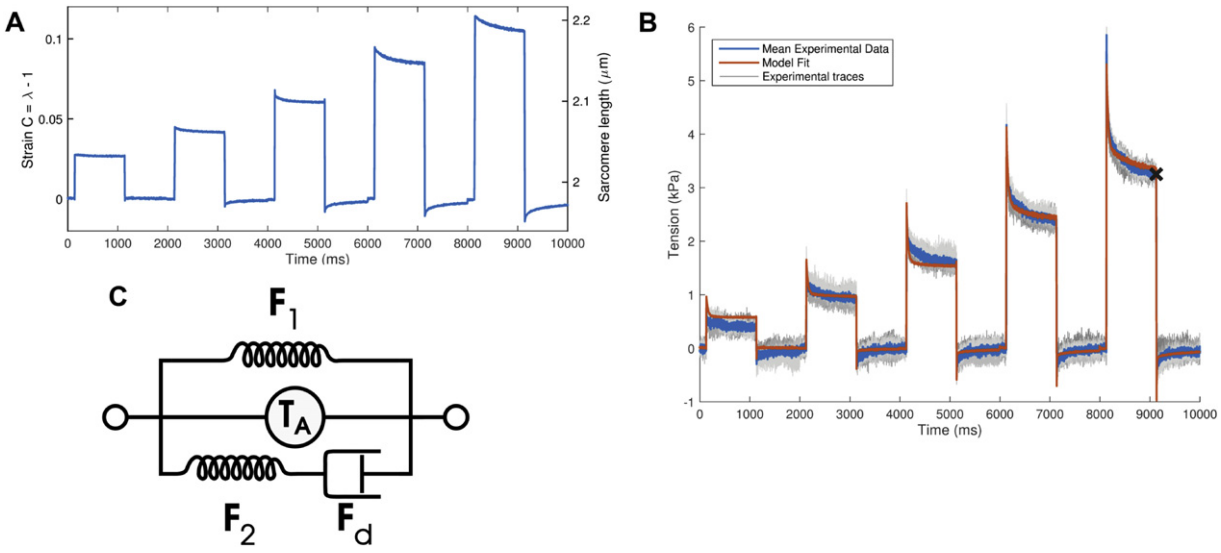

Fig. 2. Passive tension data and model fit. Panel (A) shows the mean sarcomere length measurement. Panel (B) shows passive tension data and model fit. Grey traces show $n = 7$ individual data traces, normalized to match the mean value at the black 'X'. The blue trace indicates the mean passive tension, and the red trace is our model fit. Panel (C) shows the model we use for the viscoelastic response, which is similar to a standard linear solid. F_1 is a spring with an exponential stress-strain relationship, F_2 is a linear spring, and F_d a dashpot. The active contractile element T_A is introduced in later sections, and has zero stiffness in the model fitting to passive tension data.

$$F_1 = a(e^{bC} - 1) \qquad \text{(parallel elastic element)} \qquad (3)$$

$$F_2 = akC_s \qquad \text{(series elastic element)} \qquad (4)$$

$$F_d = \begin{cases} a\eta_l \frac{dC_d}{dt} \frac{dC_d}{dt} > 0 \\ a\eta_s \frac{dC_d}{dt} \frac{dC_d}{dt} < 0 \end{cases} \qquad \text{(viscous dashpot element)} \qquad (5)$$

$$C_s + C_d = C \qquad \text{(series strain constraint)} \qquad (6)$$

$$F_2 = F_d \qquad \text{(series force constraint)} \qquad (7)$$

$$F_{\text{tot}} = F_1 + F_2 = F_1 + F_d \qquad \text{(total force)} \qquad (8)$$

Note that the parameter a is included in all forces, such that rescaling total passive force can be accomplished by a single parameter change. The resting sarcomere length SL_0 is estimated using the average of the early part of the experimental SL trace for each cell, before the first stretch. We first fit the serial spring's stiffness as $a \cdot k = 14$ to match the peaks of the viscous response. Next, we fit the remaining model parameters a, b, η_l, and η_s to the mean normalized experimental force of our cellular data, minimizing $S = \int \|F_{\text{tot}} - F_{\text{exp}}\|^2$ where F_{exp} is the experimental mean force. Parameters were rounded to a number of significant digits reflecting the sensitivity of parameters to the cost function, by rounding each parameter in turn, while keeping the minimization criterion S within 0.2% of the optimal value.

Final parameters are $a = 2.1$ kPa, $b = 9.1$, $k = 7$, $\eta_l = 200$/ms, and $\eta_s = 20$/ms, reflecting relatively low sensitivity to the viscous forces, and higher sensitivity of the passive tension parameters a and b. Fig. 2 shows experimental data and model fit.

3.2. Active tension model

In this section we develop our active tension model and fit it to our human cardiomyocytes data on steady-state force development, length dependence of this force development, and dynamic changes in tension due to fast changes in cell length.

The force generating apparatus of the cell consists primarily of two types of filaments, thick filaments and thin filaments. Thin filaments are composed of actin, tropomyosin, and troponins, including troponin C and troponin I. Thick filaments are made up of myosin crossbridges [5,18,46,60,61]. Active tension is generated by myosin crossbridges attaching to binding sites on actin on the thin filament, and then performing a *powerstroke*. Crossbridges consist of a head region which rotates during a powerstroke, and a tail region (the neck region of the myosin molecule) which is distorted. The restoring forces on the spring-like tail are responsible for force generation. As the filaments slide past each other, the distortion of the crossbridge tail which was generated by the powerstroke is reduced, generating less force. By detaching, returning to their resting length, and re-attaching to a new binding site and once again performing a powerstroke, crossbridges restore their maximal force generating ability. In the resting state, tropomyosin, which winds helically around actin on the thin filament, sterically blocks the binding sites for myosin on actin. It is held in this 'blocking' position by troponin I, another thin filament protein. When the cell is electrically activated, the calcium concentration rises. Calcium ions (Ca^{2+}) from the cytosol bind to the regulatory binding site on troponin C. This causes troponin C to open a binding pocket for troponin I, causing troponin I to preferentially move away from holding tropomyosin in the 'blocked' position, allowing crossbridges to bind and generate tension.

Our goal is to develop a model of active contraction in the human heart with a level of complexity that reflects the available experimental data, and which can be efficiently used in multi-scale cardiac mechanics models. Therefore we choose a strategy based on a low-dimensional set of ordinary differential equations, and avoid techniques based on partial differential equations [65] or very high-dimensional ODE models [8,36].

The model definition in the following sections is based on the different contractile proteins. Firstly, we describe our model for thin filament kinetics, involving troponin and tropomyosin. Secondly, we develop a model of the crossbridge cycle, including distortion-decay kinetics related to changes in length of the cell. Finally, we introduce a model of the length-dependence of tension in cardiac cells. An overview of the active contraction model is shown in Fig. 3.

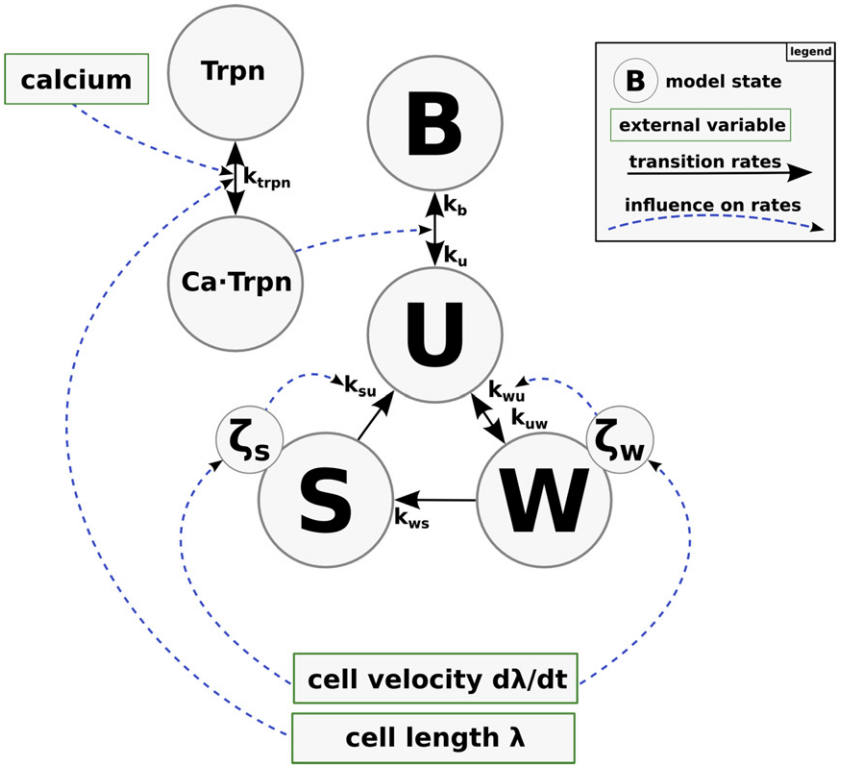

Fig. 3. Overview of the active tension model. States included the 'blocked' state 'B', the unbound crossbridge state 'U', the pre-powerstroke state 'W' and the force-generating state 'S'. Both the states 'W' and 'S' have an additional state ζ_w and ζ_s keeping track of the mean distortion of crossbridges in this state. Calcium binding to troponin C (Trpn) drives the transition between states 'B' and 'U'.

3.2.1. Thin filament kinetics

Thin filament kinetics are described by the interactions of calcium ions, troponin C, troponin I and tropomyosin to regulate availability of myosin binding sites on actin. Activation of the thin filaments shows highly cooperative behaviour, with small changes in intracellular calcium leading to potentially high changes in force. The main biophysical reason for this behaviour relates to the end-to-end overlap of tropomyosin molecules. Explicitly capturing these interactions between neighbouring molecules tends to require complex models [36]. We choose a relatively simple and phenomenological representation of cooperative activation, as it is better suited for applications in multiscale modelling.

With respect to troponin, our new active contraction model inherits troponin C dynamics and parameters other than calcium sensitivity from previous murine work [37], as these proteins are highly conserved across species [41], and we do not have new experimental data to constrain most of the parameters:

$$\frac{\mathrm{dCaTRPN}}{\mathrm{d}t} = k_{\mathrm{TRPN}} \left(\left(\frac{\left[\mathrm{Ca}^{2+}\right]_{\mathrm{i}}}{\left[\mathrm{Ca}^{2+}\right]_{\mathrm{T50}}} \right)^{n_{\mathrm{TRPN}}} (1 - \mathrm{CaTRPN}) - \mathrm{CaTRPN} \right) \tag{9}$$

where CaTRPN represents the fraction of troponin C units with calcium bound to its regulatory binding site. The parameter $k_{\mathrm{TRPN}} = 0.1/\mathrm{ms}$ represents the unbinding rate, $n_{\mathrm{TRPN}} = 2$ the cooperativity of the calcium-troponin C binding rate. The parameter $[\mathrm{Ca}^{2+}]_{\mathrm{T50}}$, which describes the half-activation point, is not consistent between species. This parameter needs to be fit depending on the calcium transient used to drive the model, and will be fit to experimental data below. The troponin concentration CaTRPN drives the unblocking of tropomyosin, as represented by the fraction of *blocked* myosin binding sites on actin, denoted by B:

$$\frac{\mathrm{d}B}{\mathrm{d}t} = k_{\mathrm{b}} \cdot \mathrm{CaTRPN}^{-n_{\mathrm{Tm}}/2} \cdot U - k_{\mathrm{u}} \cdot \mathrm{CaTRPN}^{n_{\mathrm{Tm}}/2} \cdot B \tag{10}$$

where U is the fraction of unblocked myosin binding sites without crossbridges bound. The equation for $\frac{\mathrm{d}B}{\mathrm{d}t}$ is similar to those used in previous work [37,56], giving a cooperative Hill curve with coefficient n_{Tm} as the steady-state relation between CaTRPN and the fraction of unblocked binding sites $1 - B$. For numerical stability, the term $\mathrm{CaTRPN}^{-n_{\mathrm{Tm}}/2}$ is limited to a maximum value of 100.

3.2.2. Crossbridge model

Crossbridge binding and force generation are modelled using a three-state crossbridge cycle with unbound (U), pre-powerstroke (W) and post-powerstroke (S) states, and a distortion-decay model which tracks the average distortion of crossbridges in the W and S states.

$$U = (1 - B) - S - W \tag{11}$$

$$\frac{\mathrm{d}W}{\mathrm{d}t} = k_{\mathrm{uw}} U - k_{\mathrm{wu}} W - k_{\mathrm{ws}} W - \gamma_{\mathrm{wu}} W \tag{12}$$

$$\frac{\mathrm{d}S}{\mathrm{d}t} = k_{\mathrm{ws}} W - k_{\mathrm{su}} S - \gamma_{\mathrm{su}} S \tag{13}$$

Here γ_{wu} and γ_{su} are distortion-dependent unbinding rates of crossbridges in the W and S state, given by a distortion-decay model [14,55]. We use a relatively simple distortion-decay model, inspired by the work of Ford et al. [14], Razumova et al. [55], and Rice et al. [56]. These models assume crossbridges are linearly elastic,

and tension is generated by both distortion induced by the powerstroke, and distortion induced by imposed changes in cell length. This induced distortion then decays over time as crossbridges unbind and reattach in an undeformed state. In addition, the distorted crossbridges are more likely to unbind. Although more distortion-dependent binding rates have been suggested [56], we only use an increase in crossbridge unbinding rates due to distortion. This captures the most salient features of our experimental data, notably the 'dip' in tension after a stretch, with a limited number of parameters. We also avoid exponential functions in these dependencies, as they can lead to increased stiffness of the resulting equations, and potential instability when applied in a multiscale modelling setting.

Our distortion-decay model is given by

$$\frac{d\zeta_w}{dt} = A_w \frac{d\lambda}{dt} - c_w \zeta_w \tag{14}$$

$$\frac{d\zeta_s}{dt} = A_s \frac{d\lambda}{dt} - c_s \zeta_s \tag{15}$$

$$\gamma_{wu} = \gamma_w |\zeta_w| \tag{16}$$

$$\gamma_{su} = \begin{cases} \gamma_s(-\zeta_s - 1) & \text{if} \quad \zeta_s + 1 < 0 \\ \gamma_s \zeta_s & \text{if} \quad \zeta_s + 1 > 1 \\ 0 & \text{otherwise} \quad (\text{if } \zeta_s + 1 \in [0,1]) \end{cases} \tag{17}$$

where A_w and A_s relate to the magnitude of the instantaneous response to distortion, and c_w and c_s to the decay rate of distortion. All variables with the subscript 'w' relate to the pre-powerstroke state W, and variables with the subscript 's' relate to the post-powerstroke state S. The variable λ indicates the cell length relative to the resting length [37].

Like previous models, we assume that crossbridges bind with zero distortion (not generating any tension) in the pre-powerstroke state. Furthermore, when making a powerstroke (transition from W to S), crossbridges do not retain their distortion, but end up with exactly the distortion induced by the powerstroke. This greatly simplifies the equations, without significantly impacting model results, as distortion in the W state quickly decays. Unlike some previous models [55], the distortion ζ_w and ζ_s in our model are given relative to the powerstroke distortion, with $\zeta_w = 0$ indicating no distortion, and $\zeta_s = 0$ indicating no additional distortion to that given by the powerstroke.

In the absence of changes in cell length, we have $\zeta_w = \zeta_s = 0$, and the total active tension is given by

$$T_a = \text{number of crossbridges} \times \text{crossbridge stiffness} \times \text{powerstroke distortion} \times S \tag{18}$$

When considering the distortion in both the W and S states, the total tension is proportional to

$$T_a \sim ((\zeta_s + 1) S + \zeta_w W) \tag{19}$$

The distortion-dependent unbinding term has already been incorporated in the equations for $\frac{dW}{dt}$ and $\frac{dS}{dt}$ (Eqs. (12), (13)). In the pre-powerstroke state, the distortion-dependent unbinding rate γ_{wu} is taken as proportional to distortion ζ_w. For the post-powerstroke state we assume the absence of significant distortion-dependent unbinding for any strain between the normal pre-powerstroke and post-powerstroke states, i.e. for $\zeta_s + 1 \in [0,1]$. For ζ_s outside this range, distortion-dependent unbinding scales as the absolute distance to this range, as represented by Eq. (17). This is based on both the unbinding functions proposed in Huxley-type models [25,65], and the observation that recovery after a 2% shortening step is monotonic (Fig. 5), while including significant distortion-dependent unbinding for $\zeta_s + 1 \in [0,1]$ results in non-monotonic recovery,

In a cycle of reactions, such as in our crossbridge model, it is typically easier to parameterize based on the steady-state occupation of states, and an overall rate of cycling, which governs both forward and backward rates. The steady-state occupation can be more easily constrained using a prior or fixed value, as it is less species-dependent, while the overall rate of cycling governs the kinetics of tension development, and is likely to vary significantly between species.

Thus, we introduce the following definitions:

$$r_s = \text{steady-state duty ratio} = \text{steady-state} \frac{S}{U + W + S} \tag{20}$$

$$r_w = \text{steady-state ratio between pre-powerstroke and non-strongly bound} = \text{steady-state} \frac{W}{U + W} \tag{21}$$

$$\text{TRPN}_{50} = \text{value of CaTRPN where } B = 0.5 \text{ in steady-state} \tag{22}$$

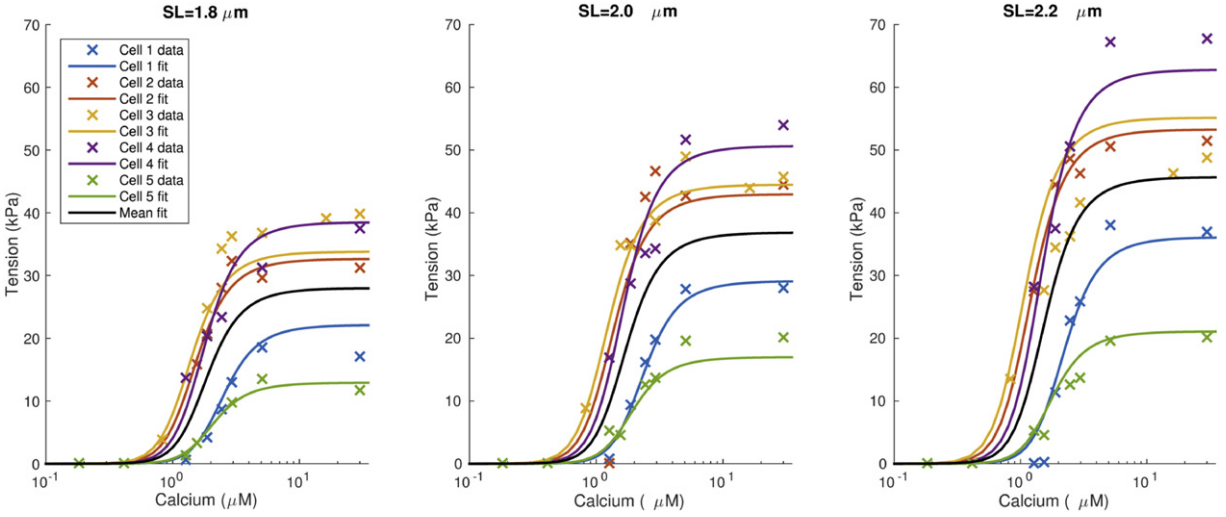

Fig. 4. Fitting cooperative activation of the model. The 'x' indicate experimental data points, with lines indicating fits to individual cells. The black line indicates the resulting mean fit.

The introduction of these variables aids in parametrization of the model as it is easier to provide a good initial estimate for r_s, r_w and TRPN_{50}, compared to directly estimating k_b, k_{su} and k_{wu}. We fix the duty ratio at $r_s = 0.25$ as in previous modelling, and consistent with experimental values for a myosin dimer [8,36]. Secondly, we have found both TRPN_{50} and r_w to be not well constrained by experimental data, with a range of values giving similar model fits. Thus, we keep $\mathrm{TRPN}_{50} = 0.35$ at the value introduced in previous work [37], which results in a peak isometric twitch tension between 1/3 and 1/2 of maximal tension, leaving potential for a strong length-dependent response. We fix $r_w = 0.5$ in the middle of the range of [0.25,0.75] we have found to fit experimental data. The derived parameters used in the model equations are given by

$$k_{wu} = k_{uw}(1/r_w - 1) - k_{ws} \tag{23}$$

$$k_{su} = k_{ws} r_w (1/r_s - 1) \tag{24}$$

$$k_b = k_u \mathrm{CaTRPN}^{n_{Tm}} / (1 - r_s - (1 - r_s) r_w) \tag{25}$$

In addition, the magnitude of instantaneous distortion in the W and S states are assumed to be equal as they reflect the distortion induced by relative movement of the filaments.

$$A_s = A_w = A_{\mathrm{eff}} \cdot r_s / ((1 - r_s) r_w + r_s) \tag{26}$$

The assumption of $A_s = A_w$ reduces the number of parameters to be estimated by one. The rescaling using A_{eff} more accurately reflects the instantaneous stiffness due to distortion, i.e. the size of the peaks in tension after a quick stretch is reflected by A_{eff} alone, independent of the choice of r_s, r_w.

Next, we assume distortion decay rates to be proportional to steady-state crossbridge cycling rates:

$$c_w = \phi \cdot k_{uw} \cdot U/W = \phi \cdot k_{uw} \cdot ((1 - r_s)(1 - r_w)) / ((1 - r_s) r_w) \tag{27}$$

$$c_s = \phi \cdot k_{ws} \cdot W/S = \phi \cdot k_{ws} \cdot ((1 - r_s) r_w) / r_s \tag{28}$$

This definition effectively eliminates a parameter by reducing two parameters (c_w, c_s) to one (ϕ). Specifically, as we assume new crossbridges enter a state with zero distortion, and unbind with average distortion, we expect the distortion decay rates are proportional to the relative increase in the state (e.g. $c_s \sim k_{ws} W/S$, as $k_{ws} W$ is the increase in S from the W to S transition). This approach is described in more detail in previous work using distortion-decay models [55,56].

3.2.3. Length-dependence of tension

Another key aspect of tension generation in the heart is the increase in generated force with an increase in cell length. At the organ level, this phenomenon gives rise to the 'Frank-Starling' effect, where an increase in end-diastolic volume leads to an increase in the volume of blood ejected, ensuring a balance of flow in and out of the heart. The molecular mechanisms underlying these effects have not been fully resolved [10].

We use a phenomenological model to represent the cellular effects, which are characterized by a shift in the sensitivity to intracellular calcium, and an increase in maximum generated tension with length [1,16,17,21]. These effects are each represented by a single parameter, as in previous work:

$$\left[\mathrm{Ca}^{2+}\right]_{T50} = \left[\mathrm{Ca}^{2+}\right]_{T50}^{\mathrm{ref}} + \beta_1 (\min(\lambda, 1.2) - 1) \tag{29}$$

$$h(\lambda) = \max(0, h'(\min(\lambda, 1.2)) \tag{30}$$

$$h'(\lambda) = 1 + \beta_0 (\lambda + \min(\lambda, 0.87) - 1.87) \tag{31}$$

The parameter β_0 represents the change in maximal tension, based on changes in filament overlap [37,56]. The parameter β_1 captures the change in calcium sensitivity [37].

Total active tension of the complete model is given by

$$T_a = h(\lambda) \frac{T_{\mathrm{ref}}}{r_s} ((\zeta_s + 1) S + \zeta_w W) \tag{32}$$

where T_{ref} is the maximal active tension at resting length. This equation results in active tension being equal to T_{ref} when $S = r_s$, as is expected at maximal calcium, when $B = 0$.

3.3. Steady-state force-pCa and length-dependent response

Measurements of the steady-state force-calcium relation for $n = 5$ cells were acquired at sarcomere length 1.8, 2.0, and 2.2 μm. Our measurements show the typical cooperative relationship between force and calcium concentration, with maximum force increasing with length, and the mid-point of activation shifting towards lower calcium levels at higher sarcomere length. Also consistent with previous work, we do not observe a change in cooperativity at this range of sarcomere lengths [28].

We use these measurements of the steady-state force-calcium relation of human cardiac myocytes to fit both cooperative activation and the length-dependent changes in both maximum force and calcium sensitivity in our model. Specifically, we fit calcium sensitivity $\left[\mathrm{Ca}^{2+}\right]_{T50}^{\mathrm{ref}}$, Hill coefficient n_H, and length-dependent parameters β_0, β_1 to the experimental dataset, using the Nelder-Mead algorithm for multidimensional unconstrained nonlinear minimization in MATLAB. Experimental data (Fig. 4) shows a degree of variability between cells, both in maximal developed tension and half-activation point. Tension is calculated as measured force divided by an estimate of cross-sectional area, therefore cell morphology and errors in cell area measurements may be the underlying cause of variations in maximum observed tension T_{ref}. The reason for variability in calcium sensitivity $\left[\mathrm{Ca}^{2+}\right]_{T50}^{\mathrm{ref}}$ is less clear, but may be related to differences in regulation of calcium dynamics due to residual phosphorylation, as a result of medication used in the process of keeping donor hearts viable. To compensate for the high variability of experimental data, we allow $\left[\mathrm{Ca}^{2+}\right]_{T50}^{\mathrm{ref}}, T_{\mathrm{ref}}$ to vary for each cell, to more accurately estimate the other parameters.

Best fit model parameters are given by $n_{Tm} = 2.2$, $\beta_1 = -2.4$, and $\beta_0 = 2.3$ with the means and standard deviations of the individually fitted parameters as $T_{\mathrm{ref}} = 40.5 \pm 14.9$ kPa and $\left[\mathrm{Ca}^{2+}\right]_{T50}^{\mathrm{ref}} = 2.5 \pm 0.66$ μM. These model results indicate a clear length-dependent maximum increase in force ($\beta_0 > 0$), with shift to higher calcium sensitivity with increased cell length ($\beta_1 < 0$). Fig. 4 shows experimental data and resulting model fits.

3.4. Velocity-dependent response

We have performed two sets of experiments relating to the acute tension response after changes in length, also known as the velocity dependence of tension. The data (Fig. 5A) shows the response of a myocyte to a quick stretch. Force increases instantly due to distortion of crossbridges, then rapidly decays and drops below the eventual steady-state tension at the increased length as distorted crossbridges detach, before recovering to a higher steady-state level of tension due to length-dependent effects [14]. Following shortening, we do not observe the biphasic force response seen after a rapid stretch. In contrast, the induced distortion causes force to decrease instantly, before recovering in a smooth, monotonically increasing manner,

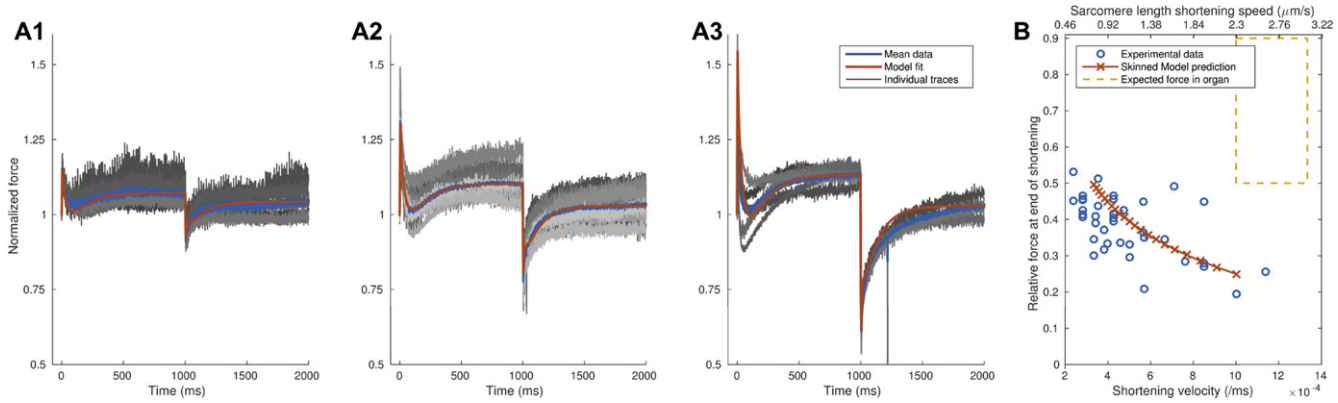

Fig. 5. Fitting velocity dependence. The three panels (A1, A2, A3) show quick stretch experiments with 0.5% stretch, 1% stretch and 2% applied in 10 ms from left to right. Grey traces are experimental data, averaging to the blue trace. Best model fit is given by the smooth red trace. Panel (B) shows constant velocity shortening experiments and results of our skinned and intact myocyte models. Raw data can be found in Appendix D. The expected force development to produce sufficient ejection in the heart is approximately 70% at constant shortening of 20% in 150–200 ms, well outside the function observed in skinned myocytes.

consistent with previous experiments [14]. In addition, we have data on constant velocity shortening, where cell length decreases by 7–11% over 100–300 ms. We combine these two data sets to select a set of model parameters k_{ws}, k_{uw}, ϕ, γ_s, and γ_w which fits both types of experimental data well. Details of the cost functions and fitting are given in Appendix C.1. Results are shown in Fig. 5.

3.5. Isometric twitch response in intact muscle

The model developed in the previous sections is constrained from data measured in skinned isolated myocytes. Skinned myocytes are known to differ from intact muscle. In particular, calcium sensitivity, cooperativity, and maximal active tension can all be significantly different [5,28]. Note that our skinned cells have a calcium sensitivity of ~3μM, while a calcium transient in an intact human myocyte (Fig. 6, left panel) has a peak calcium level of 0.6 μM. We assume intact muscle shares other properties with skinned myocytes, and differs mainly in these three parameters: calcium sensitivity $\left[Ca^{2+}\right]^{ref}_{T50}$, Hill coefficient of cooperative activation n_{Tm}, and maximal tension T_{ref}.

In this section we fit the model to isometric twitch data to capture *in vivo* function and make the model suitable for use in a multiscale cardiac mechanics modelling framework. Our experimental data is limited to skinned myocytes, as the freezing process for unused donor hearts compromises the cell membrane. Thus, we rely on published literature data to guide the parametrization of the model to represent intact muscle function. Combined force, length and calcium measurements from intact trabeculae have not been reported. Here we integrate observations of calcium transients and tension transients from different sources, to estimate the differences in parameters between skinned myocytes and intact tissue preparations

The calcium transient we use as input is based on work by Coppini et al. [9], which is shown in Fig. 6. We use isometric twitch measurements from isolated left ventricular muscle strips [44,53] at body temperature, from which we derive our target ranges for a time to peak tension (TPT) of 147–172 ms, a time to 50% relaxation (RT_{50}) of 109–125 ms and a time to 95% relaxation (RT_{95}) of 291–377 ms. These metrics along with criteria for maximal and minimal tension development are combined into a cost function and solved to result in optimized model parameters $\left[Ca^{2+}\right]^{ref}_{T50}$, n_{Tm}, k_u, as described in more detail in Appendix C.2. Resulting metrics for activation and relaxation with the optimal parameter set are a time to peak of 237 ms, relaxation times $RT_{50} = 190$ ms, $RT_{95} = 447$ ms,

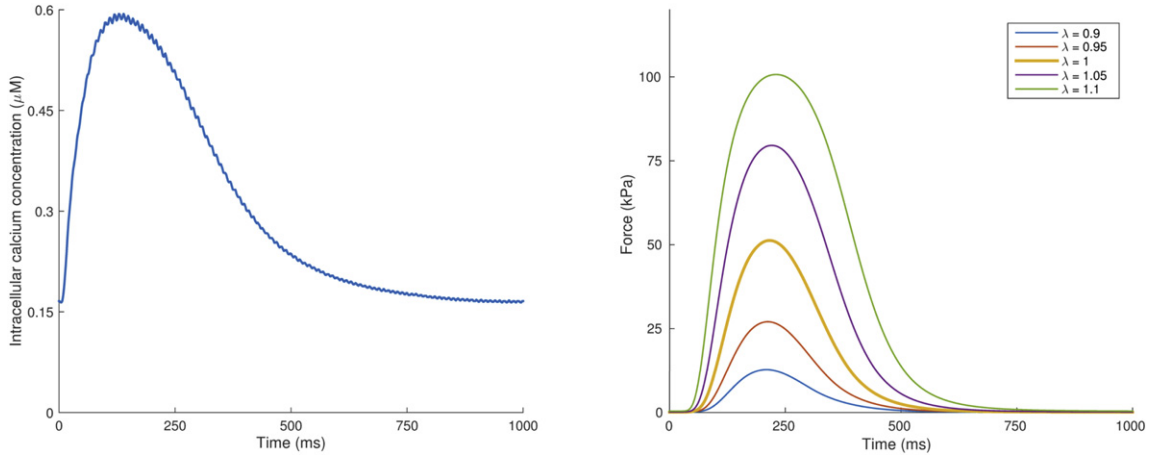

Fig. 6. Results for isometric twitch tension. The left panel shows the human calcium transient used, provided by Coppini et al. [9]. The right panel shows the isometric twitch tension produced by our model at resting length (thicker yellow line, $\lambda = 1$) and the length-dependent response at different extension ratios.

a peak tension of 34.8 kPa and a minimum tension of 0.8 kPa during 1 Hz pacing. The tension development and relaxation rates are well outside the measured ranges for isometric twitch, while the maximal tension is below that typically required to achieve a healthy ejection fraction in multi-scale simulations.

From Fig. 5A we can also see that crossbridge kinetics are slow in skinned myocytes, with recovery of tension taking several hundreds of milliseconds after 2% shortening, and Fig. 5B shows that tension development at the shortening rate observed during the fast ejection phase is expected to be well below the range compatible with a healthy ejection fraction. On the basis of these observations, we introduce additional model parameters in fitting: factor μ, which scales the weak-to-strong crossbridge transition rate k_{ws}, and ν, which scales the unbound-to-weak transition rate k_{uw}. Note that this will also affect recovery from distortion, c.f. Eq. (28). We add $\nu, \mu \in [1, 12]$ to our parameter sweep and keep other parameter ranges.

Re-running the optimization with these additional parameters results in a crossbridge rate scaling factor of $\mu = 3$, resulting in $k_{\text{ws}} = 0.012$ ms, or approximately 1/8 of the corresponding rate-limiting kinetic used in mouse modelling [37], which is consistent with the difference in heart rates between mouse and human. Other parameters fitted are $n_{\text{Tm}} = 5$, also consistent with previous modelling in intact mouse muscle, as well as with experimental data in other species [12,28,42]; $\left[\text{Ca}^{2+}\right]^{\text{ref}}_{\text{T50}} = 0.805$ μM, consistent with the magnitude of the calcium transient, and tropomyosin kinetics $k_{\text{u}} = 1$/ms at the upper bound of our parameter sweep range. Further increasing k_{u} does not significantly improve the fit, indicating the current value is near steady-state.

The parameter sweep indicated that the parameter ν, which scales the unbound-to-weak transition rate k_{uw}, could not be constrained based on twitch kinetics. Values of $\nu \in [4, 12]$ all result in insignificant differences with $d_t \in [7, 9]$, with no clear pattern of higher or lower ν consistently giving better fits. The next section describes the use of whole-organ simulations to determine this final parameter, resulting in our choice of $\nu = 7$.

Resulting metrics for activation and relaxation are a time to peak of 175 ms, relaxation times $\text{RT}_{50} = 121$ ms, $\text{RT}_{95} = 281$ ms, a peak tension of 51 kPa and a minimum tension of 0.078 kPa during 1 Hz pacing. The resulting twitch transients at different cell strains are shown in Fig. 6.

3.6. Multi-scale model

In this section we use our newly-developed single cell model of human active contraction to drive a three-dimensional finite element simulation of the heart. For use in a multi-scale context, we apply the model of active tension in an intact cell as parametrized in the previous section, and define the total tension of the cell model as

$$T_{\text{tot}} = T_a + F_d = T_a + F_2 \tag{33}$$

That is, the viscoelastic response F_d is included in the cell model. The response F_d includes titin and the effects of any residual endomysial collagen on the cells [23], but does not include the effects of thick collagen bundles which limit the operating range of the heart to a maximal sarcomere length of 2.35 μm [22], blood vessels, fibroblasts and other components of the myocardium. The constitutive law represents all of these elements in a lumped description of the passive response of myocardium. As collagen present in the heart also adds to viscosity, the term F_d may underestimate total viscosity. However, the viscous component of the model is dominated by the velocity dependence of tension, and passive viscous component has very little effect on ejection fraction. The passive elastic response F_1 (Eq. (3)) would typically be part of the constitutive law used, and should therefore not be included in the cell model when used in a multiscale context.

The minimal implementation of the passive cell model (Eqs. (1)–(8)) in this context is given by

$$T_p = F_d = F_2 = akC_s \tag{34}$$

$$C_s = (\lambda - 1) - C_d \tag{35}$$

$$\frac{\mathrm{d}C_d}{\mathrm{d}t} = kC_s/\eta \tag{36}$$

$$\eta = \begin{cases} \eta_l & C_s > 0 \\ \eta_s & C_s \leq 0 \end{cases} \tag{37}$$

where the extension ratio λ is calculated from the fibre strain $|\mathbf{Ff}|$, where $\mathbf{F}$ is the deformation gradient and $\mathbf{f}$ a unit vector in the fibre direction. A rule-based fibre direction was used, ranging from -60° at the epicardium to $+80^\circ$ at the endocardium.

Three anonymised CT data sets were obtained from patients at St Thomas' Hospital in London for diagnostic purposes, but who were all found to have healthy heart function. CT images were ECG gated for the R wave, giving the heart anatomy at end diastole. Each data set was segmented using the Philips heart atlas based segmentation tool [13]. We use the meshing tool developed by Lamata et al. [32,33] to fit a cubic order finite element mesh to each segmented data set. Fig. 7C shows the resulting finite element meshes. To simulate biventricular cardiac function, we use our multi-scale cardiac mechanics framework [34,38], which has recently been verified [35].

The constitutive law of Guccione et al. was used to represent the material [20]:

$$W = \frac{C_1}{2}(e^Q - 1) \tag{38}$$

$$Q = C_2E_{11}^2 + C_3\left(E_{22}^2 + E_{33}^2 + E_{23}^2 + E_{32}^2\right) + C_4\left(E_{12}^2 + E_{21}^2 + E_{13}^2 + E_{31}^2\right) \tag{39}$$

where W is the strain energy function and E_{ij} are components of the Green-Lagrange strain tensor $\mathbf{E}$ in a fibre-based coordinate system [35]. We use parameters $C_2 = 8$, $C_3 = 3$, $C_4 = 4$ based on Nasopoulou et al. [48] and $C_1 = 1$ kPa to match end-diastolic volume. Meshes were 'deflated' to the reference configuration using the backward displacement method [6]. Simulations were initiated by inflating the reference configuration back to end-diastolic pressure. Left-ventricular end-diastolic pressure was set to 1 kPa (7.5 mm Hg). Active contraction was driven by a prescribed calcium transient, as shown in Fig. 6, which was applied homogeneously throughout the geometry. During isovolumetric contraction, volume in the respective ventricle was held constant by solving $\frac{\mathrm{d}V}{\mathrm{d}t} = 0$ as a constraint within the system of mechanics equations. Aortic pressure at start of ejection was set to $p_a = 9$ kPa (67.5 mm Hg). When the left ventricular pressure reaches this point, ejection is started. Hemodynamics during ejection were simulated using a standard three-element windkessel model, with left-ventricular parameters $R = 0.852$ mm Hg s/ml, $C = 2.73$ ml/mm Hg, $Z = 0.035$ mm Hg s/ml based on data from Murgo et al. [45]. When during the solution process we notice a reversal in flow direction $\left(\frac{\mathrm{d}V}{\mathrm{d}t} < 0\right)$, the ejection phase ends, and the isovolumetric relaxation phase of the solver is started. This phase continues until the pressure reaches 0.1 kPa, at which point the model moves into diastole. A simple diastole model is used, which serves to return the ventricles to end-diastolic pressure, given by $\frac{\mathrm{d}p}{\mathrm{d}t} = 0.01(p - EDP)$. Right-ventricular end-diastolic

pressure was set to 1/3 of left ventricular pressure [26], and windkessel parameters were set in accordance with an approximate 1 : 3 pressure difference, i.e. $C_{\mathrm{rv}} = 3C$, $Z_{\mathrm{rv}} = Z/3$, $R_{\mathrm{rv}} = R/3$, and $p_{a,\mathrm{rv}} = 3$ kPa. Right ventricular diastolic filling was started at the same time as left ventricular diastolic filling.

3.6.1. Whole organ simulations

To confirm changes between skinned and intact myocytes, we also perform whole organ simulations $\mu = \nu = 1$. This results in ejection fractions of 20–25%, confirming the need to increase crossbridge cycling rates. We test the optimal parameter set for isometric twitches for $\mu = 3$ and ν between 1 and 12. Ejection fraction for each case is shown in Fig. 7A, and shows a steeply increasing ejection fraction until approximately $\nu = 7$. Based on these results, we choose $\nu = 7$, or $k_{\mathrm{uw}} = 0.182$ and $\left[\mathrm{Ca}^{2+}\right]^{\mathrm{ref}}_{\mathrm{T50}} = 0.805$ μM. Fig. 7B shows the pressure-volume loops of the final models representing intact and skinned myocytes, with a clear difference in ejection and pressure development.

4. Discussion

In this manuscript we presented a comprehensive data set characterizing the passive tension and active contractile properties of skinned human cardiac myocytes at body temperature, and used it to develop a novel multi-scale computational model of the human heart.

The viscoelastic properties of cardiac cells are complex and involve folding and unfolding of titin [43], with a contribution from the deformation of the cell membrane and cytoskeleton. However, we found that an efficient single ODE model, similar to that of a standard linear solid, fits our data on passive tension of cardiac myocytes, and has only five parameters. For active tension, we used a framework for troponin C kinetics from previous modelling work, but separated tropomyosin and crossbridge kinetics into separate equations. This allowed us to introduce a three-state crossbridge model, with a distortion-decay model for the velocity-dependence of cardiac muscle.

The choices made in the final modelling framework give some implicit mechanistic insights. A major motivation for introducing these extensions was the observation that the fading memory model [24] used in some of our previous work [37,49] did not accurately predict the response to shortening observed in our experimental data. Specifically, the model gives a mirrored response to shortening versus lengthening, and can not reproduce the monotonic recovery observed after shortening (Fig. 5). This inspired the development of a new model, extending the framework of Ford et al. [14], which captures the asymmetric response to fast shortening and stretch. However, as crossbridge transition rates affect the tension response to changes in cell length, the model parameters are less independent of other equations than in the fading memory model. Separating tropomyosin and crossbridge kinetics fits with this modelling approach, as it allows adding distortion-dependent unbinding rates (as reflected by γ_s and γ_w) to crossbridge states, rather than

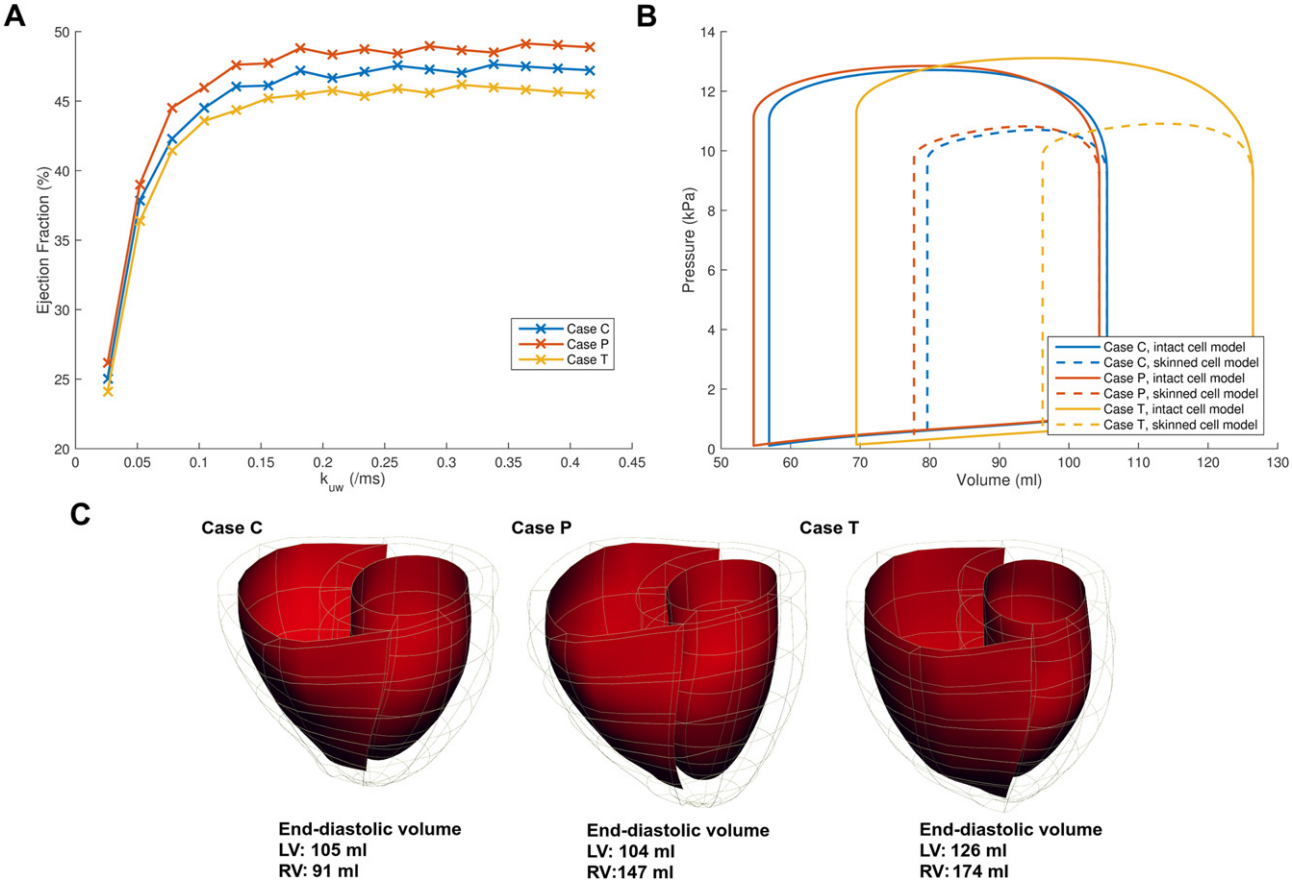

Fig. 7. Ejection fraction and pressure-volume loops. Panel (A) shows the change in ejection fraction as a function of the unbound-to-weak crossbridge binding rate for each of our three patient cases, showing stronger constraints ($k_{\mathrm{uw}} > 0.18$) than those found in isometric twitch fitting ($k_{\mathrm{uw}} > 0.078$), as well as small differences in ejection fraction between the three cases. Panel (B) shows pressure-volume relations for the original skinned model, and adjustment to crossbridge cycling rates using inferred parameters based on isometric twitch tension and ejection fraction. Panel (C) shows our three patient-specific meshes derived from CT scans, at their end-diastolic configuration.

distortion influencing tropomyosin kinetics directly. In addition, a two-state crossbridge model did not capture distortion-decay kinetics accurately, while a three-state model captures a fast component (due to weakly attached crossbridges) and a slower component (due to strongly attached crossbridges) in tension recovery.

Fitting the steady-state force-calcium relationship at different sarcomere lengths revealed a relatively low Hill coefficient in skinned myocyte data, as has been observed previously in skinned cells [5]. As expected from previous work, we found skinned cell data was not compatible with measurements of isometric twitch measurements. Specifically, calcium sensitivity in skinned cells predicts a half-activation value of approximately 3 μM, which results in near-zero isometric twitch tension based on calcium data measurements from Coppini et al., which have a peak value below 1 μM [9]. Thus, fitting isometric twitch data required differences in cooperativity and calcium sensitivity. Although direct measurements of the force-calcium response in intact cells would have helped to constrain these differences, the source of our experimental data consists of snap-frozen tissue, in which an unknown proportion of the myocytes will have been unavoidably permeabilised. Compared to experimental data, the RT_{50} values predicted by the model are at the higher end of experimental data, and RT_{95} values are at the lower end, similar to previous isometric twitch fitting in human models [36]. It remains to be seen if this difference is due to the limited measurement data available, or is a particular feature of human cardiac myocytes. Tropomyosin kinetics were best fit with a rate constant near steady-state, which suggests that tension development in humans is rate-limited by crossbridge kinetics, consistent with recent consensus on rate-limiting kinetics in cardiac tension generation [61].

A limitation of skinned myocytes which, to our knowledge, has not previously been recognized, is the slower crossbridge kinetics. Specifically, modelling predicts that crossbridge cycling rates are higher in intact myocytes compared to skinned myocytes at body temperature. As a result, in skinned myocytes recovery from shortening-induced distortion of crossbridges happens on a time scale of around 1 s which is too slow to allow for a healthy ejection fraction. Increasing the weak-to-strong crossbridge cycling rate produced a model consistent with isometric twitch data. The unbound-to-weak transition rate could not be exactly determined, but a more specific lower bound to this parameter was found by using whole organ simulations, and the final intact cell model produced a healthy ejection fraction. The weak-to-strong transition rate is estimated at approximately three times higher in intact compared to skinned myocytes based on twitch kinetics, and the unbound-to-weak transition rate at least seven times higher based on a combination of isometric twitch results and ejection fraction. The resulting crossbridge cycling rates are $r_s k_{su} = 6$/s in the skinned model and $\mu = 3$ times higher (18/s) in the intact model. The cycling rate in skinned cells in the model is approximately twice that of an estimate derived from ATPase measurements at lower temperature in human skinned muscle strips of 3/s, based on a myosin ATPase activity in skinned human preparations of 50 μM/s at 20 °C [47], a myosin S1 concentration of 157 μM [4], and a Q_{10} of 3.5 [11].

These differences are potentially related to the swelling of the myofilament lattice as a result of the skinning process. Such increased distance between thick and thin filaments would be expected to change the attachment rate and weak-to-strong transition rate of crossbridges. We attempted to prevent the lattice expansion by using 3% dextran T500 in the solutions. However, in our current experimental setup this led to very slow flow of solutions through the bath perfusion pipette and prevented proper activation of the myocytes.

The parameters in the model of tension generation in the skinned myocyte were revised to capture the distinct changes in tension kinetics observed in intact trabeculae experiments. Which parameters to change between skinned and intact myocytes is a choice that depends on a balance of physiological plausibility and effectiveness in reproducing the observed differences. The main kinetic parameters relate to troponin C, tropomyosin, and crossbridge cycling. Of these, we did not consider the parameters pertaining to troponin C and tropomyosin, because these are too fast for parameter changes to compensate for the change in tension kinetics between skinned and intact preparations. Thus, crossbridge rates are a natural target for consideration. The process of skinning is known to increase inter filament spacing [27], and this in turn could change the strain on the crossbridge tail. As this could affect both unbound-to-weak and weak-to-strong binding rates in a unique way, we considered these parameters first. Changing the distortion decay rates is another potentially effective option. However, as these distortion decay rate constants are related to crossbridge cycling rates, we considered this the less physiologically plausible to change these in isolation.

The changes in parameters between the models of isolated skinned myocytes and intact trabeculae raises serious questions on the underlying cause of these differences. As the experimental data on constant velocity shortening and quick stretch shows kinetics which are too slow to be compatible with healthy ejection (Fig. 5), the differences between our skinned cell data and isometric twitch kinetics are unlikely to be a modelling artefact. However, crossbridge cycling rates in models fitted to data from mouse and rat skinned trabeculae appear to be appropriate for intact whole organ simulations [62,63]. At present we do not know why the same does not hold with human skinned myocytes and whole-heart simulations. One possibility is that the attachment of myocytes to the force transducer with adhesive may introduce some end-compliance, which would slow kinetics, due to internal shortening of sarcomeres. This possibility is backed up by the small but consistent overshoot in the sarcomere strain signal (Fig. 1), with no overshoot in the length (servomotor) signal, which is consistent with compliance in the adhesive allowing the sarcomeres in the myocyte to shorten a little after the stretch. Previously we found no overshoot of SL in similar experiments at 15 °C [23]. Another possibility is that subtle damage to sarcomere structure occurs during the standard method for freezing/thawing of the cardiac tissue, or during subsequent cell isolation procedure. Overall, our initial hypothesis that skinned cardiac myocytes have crossbridge dynamics consistent with intact cells in whole organ function appears to be incorrect, at least in the narrow sense of our particular cells and experimental methods. Higher availability of human myocytes to different research groups, and refinement of techniques used to study their function at body temperature, would help research in this area. Particularly, the cells used are a scarce resource, and measurements at body temperature introduce new difficulties in experimental protocol. We have chosen to generate a range of different experiments to parameterize a simple, but complete computational model, rather than focus on generating the highest possible sample size for one particular experiment.

As with any complex multi-physics model, our approach has a number of potential limitations. The cell model does not represent a complete description of all know tension regulatory mechanisms and its complexity is motivated by the available experimental data. Specifically, feedback from force generation on Ca^{2+} affinity for troponin C, while observed experimentally [29], was not included in the model for three reasons. Firstly, during the tension transient, peak tension occurs during the decay phase of calcium transient, thus the effect of tension will be limited to the latter phases of the calcium transient. Secondly, including direct feedback from the *S* or *W* states on troponin C calcium affinity using a simple global feedback term typically leads to hysteresis [57] and has the potential for failure to relax in a multi-scale modelling setting. Finally, the collected human cardiac experimental data is not sufficiently detailed to

constrain this effect. We model these effects only as a direct length-dependence of calcium sensitivity, disregarding more complex interactions, to optimize the model in representing normal physiological function. Our multi-scale model shows slower relaxation of the pressure transient in isovolumetric relaxation than typically observed in clinical measurements. This is related to the significant difference in relaxation time in whole-organ experimental data as compared to isometric twitch data. A potential solution which was recently proposed [7] involves the modelling of internal shortening, which may extend the duration of tension generation, and improve subsequent relaxation. However, this modelling approach is currently not adapted to an ODE based framework and requires additional parameters for the hypothetical mechanism. Our model does not include beta-adrenergic stimulation, which may create disparities between cellular and whole-organ conditions, although these are expected to be relatively small under basal conditions.

In conclusion, we have presented a comprehensive new data set on contractile function in human cardiomyocytes at body temperature. The computational model developed from this data set can be used to drive a range of new computational research into human cardiac function. Model equations, parameters, and UNIPROT codes corresponding to model proteins are provided in the appendix[1].

Funding

This work was supported by the Biotechnology and Biological Sciences Research Council grant BB/J017272/1, the Engineering and Physical Sciences Research Council grant EP/M012492/1 (S.A.N.), and the Department of Health via the National Institute for Health Research (NIHR) comprehensive Biomedical Research Centre award to Guy's & St Thomas' NHS Foundation Trust in partnership with King's College London and King's College Hospital NHS Foundation Trust.

Acknowledgments

The authors thank Dr Rafaelle Coppini for providing the data for human calcium transients.

Appendix A. Model equations

The model of passive and viscoelastic tension development consists of a single ordinary differential equation

$$\frac{dC}{dt} = \frac{d\lambda}{dt} - 1 \tag{40}$$

$$F_1 = a(e^{bC} - 1) \quad \text{(parallel elastic element)} \tag{41}$$

$$F_2 = akC_s \quad \text{(series elastic element)} \tag{42}$$

$$F_d = \begin{cases} a\eta_l \frac{dC_d}{dt} & \frac{dC_d}{dt} > 0 \\ a\eta_s \frac{dC_d}{dt} & \frac{dC_d}{dt} < 0 \end{cases} \qquad \text{(viscous dashpot element)} \tag{43}$$

$$C_s + C_d = C \quad \text{(series constraint)} \tag{44}$$

$$F_2 = F_d \quad \text{(series constraint)} \tag{45}$$

$$F_{\text{tot}} = F_1 + F_2 = F_1 + F_d \quad \text{(total tension)} \tag{46}$$

The model of active tension development consists of six ordinary differential equations:

$$\frac{d\text{CaTRPN}}{dt} = k_{\text{TRPN}} \left(\left(\frac{\left[\text{Ca}^{2+}\right]_i}{\left[\text{Ca}^{2+}\right]_{\text{T50}}} \right)^{n_{\text{TRPN}}} (1 - \text{CaTRPN}) - \text{CaTRPN} \right) \tag{47}$$

$$\frac{dB}{dt} = k_b \cdot \text{CaTRPN}^{-n_{\text{Tm}}/2} \cdot U - k_u \cdot \text{CaTRPN}^{n_{\text{Tm}}/2} \cdot B \tag{48}$$

$$\frac{dW}{dt} = k_{uw}U - k_{wu}W - k_{ws}W - \gamma_{wu}W \tag{49}$$

$$\frac{dS}{dt} = k_{ws}W - k_{su}S - \gamma_{su}S \tag{50}$$

$$\frac{d\zeta_w}{dt} = A_w \frac{d\lambda}{dt} - c_w\zeta_w \tag{51}$$

$$\frac{d\zeta_s}{dt} = A_s \frac{d\lambda}{dt} - c_s\zeta_s \tag{52}$$

$$T_a = \frac{T_{\text{ref}}}{r_s} (S(\zeta_s + 1) + W\zeta_w) \tag{53}$$

where:

$$\lambda = \text{SL}/\text{SL}_0 = |\mathbf{Ff}| \quad \text{(in multiscale simulations)} \tag{54}$$

$$U = (1 - B) - S - W \tag{55}$$

$$\gamma_{wu} = \gamma_w|\zeta_w| \tag{56}$$

$$\gamma_{su} = \begin{cases} \gamma_s(-\zeta_s - 1) & \text{if} \quad \zeta_s + 1 < 0 \\ \gamma_s\zeta_s & \text{if} \quad \zeta_s + 1 > 1 \\ 0 & \text{otherwise (if} \quad \zeta_s + 1 \in [0, 1]) \end{cases} \tag{57}$$

$$A_s = A_w = A_{\text{eff}} \cdot r_s/((1 - r_s)r_w + r_s) \tag{58}$$

$$k_{wu} = k_{uw}(1/r_w - 1) - k_{ws} \tag{59}$$

$$k_{su} = k_{ws}r_w(1/r_s - 1) \tag{60}$$

$$k_b = k_u\text{CaTRPN}^{n_{\text{Tm}}}/(1 - r_s - (1 - r_s)r_w) \tag{61}$$

$$c_w = \phi \cdot k_{uw} \cdot U/W = \phi \cdot k_{uw} \cdot ((1 - r_s)(1 - r_w))/((1 - r_s)r_w) \tag{62}$$

$$c_s = \phi \cdot k_{ws} \cdot W/S = \phi \cdot k_{ws} \cdot ((1 - r_s)r_w)/r_s \tag{63}$$

In the context of an isolated myocyte, total tension is given by

$$T_a + F_{\text{tot}} \tag{64}$$

In a multi-scale modelling application, only part of the viscoelastic force in the model should be included, resulting in

$$T_a + F_d \tag{65}$$

[1] See cemrg.co.uk for model implementations.

Appendix B. Model parameters

Model parameters are given by:

Parameter	Skinned model value	Whole organ model value (if different)
Passive tension model		
a	2.1 kPa	
b	9.1	
k	7	
η_l	200/ms	
η_s	20/ms	
Active tension model		
k_{TRPN}	0.1/ms	
n_{TRPN}	2	
$\left[\mathrm{Ca}^{2+}\right]^{\mathrm{ref}}_{\mathrm{T50}}$	2.5 μM	0.805 μM
k_{u}	1/ms	
n_{Tm}	2.2	5
TRPN_{50}	0.35	
k_{uw}	0.026/ms	0.182/ms
k_{ws}	0.004/ms	0.012/ms
r_w	0.5	
r_s	0.25	
γ_s	0.0085	
γ_w	0.615	
ϕ	2.23	
A_{eff}	25	
β_0	2.3	
β_1	−2.4	
T_{ref}	40.5 kPa	120 kPa

Appendix C. Cost functions used in fitting

C.1. Velocity dependence

Simulations for constant velocity shortening are faster, but also constrain fewer of the parameters, while simulations with the quick stretch protocol contain more information about crossbridge kinetics. We fit the velocity dependence model by doing a parameter sweep on the constant shortening experiments using a very simple cost function, thoroughly exploring the parameter space in an efficient manner, but not fully constraining the model. We start by fitting the cost function $d_s = 50(\parallel F_s(10\%,100) - 0.2 \parallel + \parallel F_s(10\%,200) - 0.4 \parallel + \parallel F_s(10\%,300) - 0.5 \parallel)$, where $F_s(\delta, t_e)$ is the fraction of active tension remaining after shortening by δ in t_e ms. This cost function corresponds to matching the center of the experimental data for shortening in 100, 200, and 300 ms. The ranges of the parameter sweep were set to $k_{\mathrm{ws}} \in [0.001, 0.05]$, $k_{\mathrm{uw}} \in [0.02, 1]$, $\phi \in [0.1, 4]$, $\gamma_s \in [0.005, 0.02]$, and $\gamma_w \in [0.05, 3]$ based on earlier parameters fitted to pilot data. We also tested alternative $r_w \in [0.25, 0.75]$ and $r_s \in [0.1, 0.25]$. Of the 46,656 parameter sets tested, the minimal d_s score was 8.6. We included the 2526 parameter sets with cost $d_s < 17$ in the fitting procedure for quick stretch experiments, all of which had $r_w = 0.5$ and $r_s = 0.25$. Other than $\phi > 0.2$, no hard constraints on the other parameters were found, showing that constant velocity shortening experiments in isolation do not sufficiently constrain our model parameters.

To further constrain the distortion-decay component of the model, we compared model predictions with quick stretch experimental data. To fit our distortion-decay component to the quick stretch data, our full computational model is run to steady-state to generate the steady-state initial condition, using $[\mathrm{Ca}^{2+}]_{\mathrm{i}} = 30\mu\mathrm{M}$ and $\lambda = 1$ consistent with the experimental protocol. Experimental data for velocity dependence, like those in the previous section, again show high variability in tension development. As all parameters fitted in this section relate to the relative effects of distortion on force development, we compensate for this variability by normalizing all experimental data and model runs to be relative to tension development at the start of the protocol. Small differences remain in force at the start and end of the experimental protocol, which we assume are due to lack of complete steady-state at the start of the protocol. We choose our initial model condition by picking a time point from the steady-state calculation which matches this relative force development, and allows the model to fit both of these points exactly. As we wish to focus on distortion-decay kinetics in this data, as opposed to force-length interactions, we correct for differences in length dependence by adjusting β_0 for each of the three simulations, such that the change in tension between steady-state with the change in length is exactly captured by the length dependence equation. We define a cost function $d_v = \int \left\| T_a(t) - F_e(t) \right\|^2$ between the model force and the average experimental traces. The model force includes the generation of passive force, although it contributes less than 10% to the response to a quick stretch at this level of activation. Similar to the passive tension model fitting, we start by fitting $A_{\mathrm{eff}} = 25$ to the instantaneous response in force after a quick change in length. This response is limited to a narrow region in time, and is therefore not well constrained by our cost function. Next, we test all 2526 selected parameter sets from our parameter sweep on the constant velocity shortening data described above. The d_v score for these varies between 107 and 2973, showing that including the quick stretch experiments is key in constraining parameters. We select the parameter set with minimal d_v and use this as a starting point for the Nelder-Mead minimization algorithm with the cost function $d_v + d_s$.

C.2. Isometric twitch

Our target ranges for isometric twitch are given by a time to peak tension (TPT) of 147–172 ms, a time to 50% relaxation (RT_{50}) of 109–125 ms and a time to 95% relaxation (RT_{95}) of 291–377 ms. Based on these measurements, we use the cost function:

$$\begin{aligned} d_t =& d(\mathrm{TPT}, [147, 172]) + d\left(\mathrm{RT}_{50}, [109, 125]\right) + d\left(\mathrm{RT}_{95}, [291, 377]\right) \\ &+ 10d\left(\max F, [50, \infty)\right) + 25 \min F \end{aligned} \tag{66}$$

where $F(t)$ is the twitch force over time, and $d(a, [b, c])$ is the distance from a to the range $[b, c]$, i.e. zero if $a \in [b, c]$ and the minimal absolute distance to b or c otherwise. Weights for minimal and maximal active tension were chosen to ensure good activation and relaxation as a first priority, which are particularly important for use of the cellular model to drive whole organ contraction. Maximal active tension T_{ref} is not constrained by this data and was set to 120 kPa, consistent with force required for whole organ contraction in previous work [37] and recent data [7].

In addition to the calcium sensitivity $\left[\mathrm{Ca}^{2+}\right]^{\mathrm{ref}}_{\mathrm{T50}}$ and Hill coefficient n_{Tm}, the tropomyosin rate constant k_{u} is yet to be determined. In fitting, we use a three-dimensional parameter sweep over the ranges $\left[\mathrm{Ca}^{2+}\right]^{\mathrm{ref}}_{\mathrm{T50}} \in [0.8, 0.9]$, $n_{\mathrm{Tm}} \in [3, 7]$, $k_{\mathrm{u}} \in [0.01, 2]$ to determine the parameters. Within these constraints, no suitable parameters were found, with the minimal $d_t = 462$. We introduced a factor $\mu \in [1, 12]$, which scales the weak-to-strong crossbridge transition rate k_{ws}, and $\nu in [1, 12]$, which scales the unbound-to-weak transition rate k_{uw}. Fitting using this parameter sweep approach results in a minimum $d_t = 8$, near the constraints for relaxation and activation kinetics.

Appendix D. Raw data for force-velocity experiments

Fig. 8 shows the experimental data for the constant velocity shortening experiments.

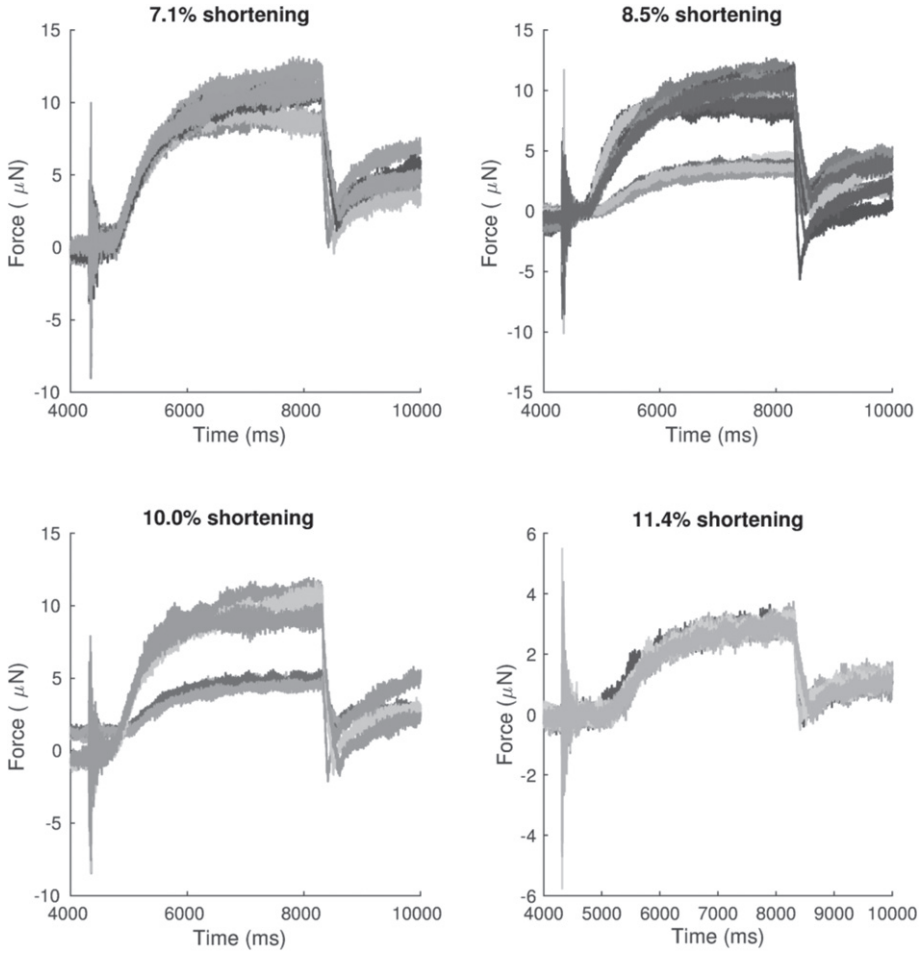

Fig. 8. Experimental data for constant velocity shortening experiments. Shown in this figure is the raw data relating to Fig. 5B.

Appendix E. UNIPROT Codes

Equations in the model are linked to contractile proteins in a human cardiac myocyte. The following table gives the corresponding UNIPROT codes for these proteins:

Model variable	Related protein	UNIPROT code
CaTRPN	Troponin C	P63316
B	Tropomyosin	P09493
B	Troponin I	P19429
B	Actin	P68032
W, S, ζ_w, ζ_s	Myosin II heavy chain	Q9UKX2
W, S, ζ_w, ζ_s	Myosin II light chain	P10916
passive model	Titin (among others)	Q8WZ42

References

[1] D. Allen, J. Kentish, The cellular basis of the length-tension relation in cardiac muscle, J. Mol. Cell. Cardiol. 17 (9) (September 1985) 821–840.
[2] C.M. Augustin, A. Neic, M. Liebmann, A.J. Prassl, S.A. Niederer, G. Haase, G. Plank, Anatomically accurate high resolution modeling of human whole heart electromechanics: a strongly scalable algebraic multigrid solver method for nonlinear deformation, J. Comput. Phys. 305 (January 2016) 622–646.
[3] B. Baillargeon, I. Costa, J.R. Leach, L.C. Lee, M. Genet, A. Toutain, J.F. Wenk, M.K. Rausch, N. Rebelo, G. Acevedo-Bolton, E. Kuhl, J.L. Navia, J.M. Guccione, Human cardiac function simulator for the optimal design of a novel annuloplasty ring with a sub-valvular element for correction of ischemic mitral regurgitation, Cardiovasc. Eng. Technol. 6 (2) (February 2015) 105–116.
[4] R.J. Barsotti, M.A. Ferenczi, Kinetics of ATP hydrolysis and tension production in skinned cardiac muscle of the guinea pig., J. Biol. Chem. 263 (32) (November 1988) 16750–16756.
[5] D. Bers, Excitation-Contraction Coupling and Cardiac Contractile Force, 2nd ed., Springer. August 2001.
[6] J. Bols, J. Degroote, B. Trachet, B. Verhegghe, P. Segers, J. Vierendeels, A computational method to assess the in vivo stresses and unloaded configuration of patient-specific blood vessels, J. Comput. Appl. Math. 246 (July 2013) 10–17.
[7] K.S. Campbell, Compliance accelerates relaxation in muscle by allowing myosin heads to move relative to actin, Biom. J. 110 (3) (February 2016) 661–668.
[8] S.G. Campbell, F.V. Lionetti, K.S. Campbell, A.D. McCulloch, Coupling of adjacent tropomyosins enhances cross-bridge-mediated cooperative activation in a Markov model of the cardiac thin filament, Biom. J. 98 (10) (May 2010) 2254–2264.
[9] R. Coppini, C. Ferrantini, L. Yao, P. Fan, M. Del Lungo, F. Stillitano, L. Sartiani, B. Tosi, S. Suffredini, C. Tesi, M. Yacoub, I. Olivotto, L. Belardinelli, C. Poggesi, E. Cerbai, A. Mugelli, Late sodium current inhibition reverses electromechanical dysfunction in human hypertrophic cardiomyopathy, Circulation 127 (5) (February 2013) 575–584.
[10] P.P. de Tombe, R.D. Mateja, K. Tachampa, Y. Ait Mou, G.P. Farman, T.C. Irving, Myofilament length dependent activation, J. Mol. Cell. Cardiol. 48 (5) 2010 851–858 PMID: 20053351.
[11] P.P. De Tombe, G.J.M. Stienen, Impact of temperature on cross-bridge cycling kinetics in rat myocardium, J. Physiol. 584 (2) (October 2007) 591–600.
[12] D.P. Dobesh, J.P. Konhilas, P.P. de Tombe, Cooperative activation in cardiac muscle: impact of sarcomere length, Am. J. Physiol. Heart Circ. Physiol. 282 (3) (March 2002) H1055–H1062.
[13] O. Ecabert, J. Peters, H. Schramm, C. Lorenz, J. v. Berg, M.J. Walker, M. Vembar, M.E. Olszewski, K. Subramanyan, G. Lavi, J. Weese, Automatic model-based segmentation of the heart in CT images, IEEE Trans. Med. Imaging 27 (9) (September 2008) 1189–1201.
[14] S.J. Ford, M. Chandra, R. Mamidi, W. Dong, K.B. Campbell, Model representation of the nonlinear step response in cardiac muscle, J. Gen. Physiol. 136 (2) (January 2010) 159–177.

[15] T. Fritz, C. Wieners, G. Seemann, H. Steen, O. Dössel, Simulation of the contraction of the ventricles in a human heart model including atria and pericardium, Biomech. Model. Mechanobiol. 13 (3)2014 627–641.

[16] F. Fuchs, D.A. Martyn, Length-dependent Ca^{2+} activation in cardiac muscle: some remaining questions, J. Muscle Res. Cell Motil. 26 (4-5) (October 2005) 199–212.

[17] N. Fukuda, T. Terui, I. Ohtsuki, S. Ishiwata, S. Kurihara, Titin and troponin: central players in the Frank-Starling mechanism of the heart, Curr. Cardiol. Rev. 5 (2) (May 2009) 119–124. PMID: 20436852 PMCID: PMC2805814.

[18] M.A. Geeves, K.C. Holmes, The molecular mechanism of muscle contraction, in: J.M. Squire, D.A.D. Parry (Eds.), Advances in Protein Chemistry, 71, Academic Press. 2005, pp. 161–193.

[19] E. Grandi, F.S. Pasqualini, D.M. Bers, A novel computational model of the human ventricular action potential and Ca transient, J. Mol. Cell. Cardiol. 48 (1) (January 2010) 112–121.

[20] J.M. Guccione, A.D. McCulloch, L.K. Waldman, Passive material properties of intact ventricular myocardium determined from a cylindrical model, J. Biomech. Eng. 113 (1) (February 1991) 42–55. PMID: 2020175.

[21] L.M. Hanft, F.S. Korte, K.S. McDonald, Cardiac function and modulation of sarcomeric function by length, Cardiovasc. Res. 77 (4) (March 2008) 627–636.

[22] P. Hanley, A. Young, I. LeGrice, S. Edgar, D. Loiselle, 3-Dimensional configuration of perimysial collagen fibres in rat cardiac muscle at resting and extended sarcomere lengths., J. Physiol. (1999) 517:Pt 3.

[23] A.C. Hoskins, A. Jacques, S.C. Bardswell, W.J. McKenna, V. Tsang, C.G. dos Remedios, E. Ehler, K. Adams, S. Jalilzadeh, M. Avkiran, H. Watkins, C. Redwood, S.B. Marston, J.C. Kentish, Normal passive viscoelasticity but abnormal myofibrillar force generation in human hypertrophic cardiomyopathy, J. Mol. Cell. Cardiol. 49 (5) (November 2010) 737–745.

[24] P.J. Hunter, A.D. McCulloch, H. Ter Keurs, Modelling the mechanical properties of cardiac muscle, Prog. Biophys. Mol. Biol. 69 (2-3) (1998) 289–331.

[25] A.F. Huxley, Muscle structure and theories of contraction, Prog. Biophys. Biophys. Chem. 7 (1957) 255–318. PMID: 13485191.

[26] E.R. Hyde, J.M. Behar, A. Crozier, S. Claridge, T. Jackson, M. Sohal, J.S. Gill, M.D. O'Neill, R. Razavi, S.A. Niederer, C.A. Rinaldi, Improvement of right ventricular hemodynamics with left ventricular endocardial pacing during cardiac resynchronization therapy, Pacing Clin. Electrophysiol. 39 (6) (June 2016) 531–541.

[27] T.C. Irving, J. Konhilas, D. Perry, R. Fischetti, P.P. de Tombe, Myofilament lattice spacing as a function of sarcomere length in isolated rat myocardium, Am. J. Physiol. Heart Circ. Physiol. 279 (5) (November 2000) H2568–H2573.

[28] J. Kentish, H. ter Keurs, L. Ricciardi, J. Bucx, M. Noble, Comparison between the sarcomere length-force relations of intact and skinned trabeculae from rat right ventricle. Influence of calcium concentrations on these relations, Circ. Res. 58 (6) (June 1986) 755–768.

[29] J.C. Kentish, A. Wrzosek, Changes in force and cytosolic Ca^{2+} concentration after length changes in isolated rat ventricular trabeculae, Am. J. Phys. 506 (2) (January 1998) 431–444.

[30] R.C.P. Kerckhoffs, P.H.M. Bovendeerd, F.W. Prinzen, K. Smits, T. Arts, Intra- and interventricular asynchrony of electromechanics in the ventricularly paced heart, J. Eng. Math. 47 (3/4) (December 2003) 201–216.

[31] N.M. King, M. Methawasin, J. Nedrud, N. Harrell, C.S. Chung, M. Helmes, H. Granzier, Mouse intact cardiac myocyte mechanics: cross-bridge and titin-based stress in unactivated cells, J. Gen. Physiol. 137 (1) (January 2011) 81–91.

[32] P. Lamata, S. Niederer, D. Nordsletten, D.C. Barber, I. Roy, D.R. Hose, N. Smith, An accurate, fast and robust method to generate patient-specific cubic Hermite meshes, Med. Image Anal. 15 (6) (December 2011) 801–813. PMID: 21788150.

[33] P. Lamata, M. Sinclair, E. Kerfoot, A. Lee, A. Crozier, B. Blazevic, S. Land, A.J. Lewandowski, D. Barber, S. Niederer, N. Smith, An automatic service for the personalization of ventricular cardiac meshes, J. R. Soc. Interface 11 (91) (February 2014) 20131023.

[34] S. Land, S.A. Niederer, N.P. Smith, Efficient computational methods for strongly coupled cardiac electromechanics, Biomed. Eng. Trans. IEEE. 59 (5) (May 2012) 1219–1228.

[35] S. Land, V. Gurev, S. Arens, C.M. Augustin, L. Baron, R. Blake, C. Bradley, S. Castro, A. Crozier, M. Favino, T.E. Fastl, T. Fritz, H. Gao, A. Gizzi, B.E. Griffith, D.E. Hurtado, R. Krause, X. Luo, M.P. Nash, S. Pezzuto, G. Plank, S. Rossi, D. Ruprecht, G. Seemann, N.P. Smith, J. Sundnes, J.J. Rice, N. Trayanova, D. Wang, Z.J. Wang, S.A. Niederer, Verification of cardiac mechanics software: benchmark problems and solutions for testing active and passive material behaviour, Proc. R. Soc. A 471 (2184) (December 2015) 20150641.

[36] S. Land, S.A. Niederer, A spatially detailed model of isometric contraction based on competitive binding of troponin I explains cooperative interactions between tropomyosin and crossbridges, PLoS Comput. Biol. 11 (8) (August 2015) e1004376.

[37] S. Land, S.A. Niederer, J.M. Aronsen, E.K.S. Espe, L. Zhang, W.E. Louch, I. Sjaastad, O.M. Sejersted, N.P. Smith, An analysis of deformation-dependent electromechanical coupling in the mouse heart, J. Physiol. 590 (18) (September 2012) 4553–4569.

[38] S. Land, S.A. Niederer, P. Lamata, N.P. Smith, Improving the stability of cardiac mechanical simulations, I.E.E.E. Trans. Biomed. Eng. 62 (3) (March 2015) 939–947.

[39] S. Land, S.A. Niederer, W.E. Louch, A.T. Røe, J.M. Aronsen, D.J. Stuckey, M.B. Sikkel, M.H. Tranter, A.R. Lyon, S.E. Harding, N.P. Smith, Computational modeling of Takotsubo cardiomyopathy: effect of spatially varying β-adrenergic stimulation in the rat left ventricle, Am. J. Physiol. Heart Circ. Physiol. 307 (10) (November 2014) H1487–H1496.

[40] S. Land, S.A. Niederer, W.E. Louch, O.M. Sejersted, N.P. Smith, Integrating multi-scale data to create a virtual physiological mouse heart, Interface Focus 3 (2). (June 2013)

[41] S.C. Little, B.J. Biesiadecki, A. Kilic, R.S.D. Higgins, P.M.L. Janssen, J.P. Davis, The rates of Ca^{2+} dissociation and cross-bridge detachment from ventricular myofibrils as reported by a fluorescent cardiac troponin C, J. Biol. Chem. 287 (33) (October 2012) 27930–27940.

[42] K.S. McDonald, R.L. Moss, Osmotic compression of single cardiac myocytes eliminates the reduction in Ca^{2+} sensitivity of tension at short sarcomere length, Circ Res 77 (1) (July 1995) 199–205.

[43] A. Minajeva, M. Kulke, J.M. Fernandez, W.A. Linke, Unfolding of titin domains explains the viscoelastic behavior of skeletal myofibrils, Biophys. J. 80 (3) (March 2001) 1442–1451.

[44] L.A. Mulieri, G. Hasenfuss, B. Leavitt, P.D. Allen, N.R. Alpert, Altered myocardial force-frequency relation in human heart failure, Circulation 85 (5) (1992) 1743.

[45] J.P. Murgo, N. Westerhof, J.P. Giolma, S.A. Altobelli, Aortic input impedance in normal man: relationship to pressure wave forms, Circulation 62 (1) (January 1980) 105–116.

[46] A. Månsson, D. Rassier, G. Tsiavaliaris, Poorly understood aspects of striated muscle contraction, Biomed. Res. Int. 2015 (April 2015) e245154.

[47] N.A. Narolska, S. Eiras, R.B.v. Loon, N.M. Boontje, R. Zaremba, S.R.S. Berg, W. Stooker, M.a.J.M. Huybregts, F.C. Visser, J. v. d. Velden, G.J.M. Stienen, Myosin heavy chain composition and the economy of contraction in healthy and diseased human myocardium, J. Muscle Res. Cell Motil. 26 (1) (February 2005) 39–48.

[48] A. Nasopoulou, B. Blazevic, A. Crozier, W. Shi, A. Shetty, C.A. Rinaldi, P. Lamata, S.A. Niederer, Myocardial stiffness estimation: a novel cost function for unique parameter identification, in: H. van Assen, P. Bovendeerd, T. Delhaas (Eds.), Functional Imaging and Modeling of the Heart, Number 9126 in Lecture Notes in Computer Science, Springer International Publishing. June 2015, pp. 355–363. http://dx.doi.org/10.1007/978-3-319-20309-6_41.

[49] S.A. Niederer, P.J. Hunter, N.P. Smith, A quantitative analysis of cardiac myocyte relaxation: a simulation study, Biophys. J. 90 (5) (2006) 1697–1722.

[50] S.A. Niederer, S. Land, S.W. Omholt, N.P. Smith, Interpreting genetic effects through models of cardiac electromechanics, Am. J. Physiol. Heart Circ. Physiol. 303 (11) (December 2012) H1294–1303. PMID: 23042948.

[51] S. Niederer, N. Smith, The role of the Frank-Starling law in the transduction of cellular work to whole organ pump function: a computational modeling analysis, PLoS Comput. Biol. 5 (4). (2009)

[52] T. O'Hara, L. Virág, A. Varró, Y. Rudy, Simulation of the undiseased human cardiac ventricular action potential: model formulation and experimental validation, PLoS Comput. Biol. 7 (5) (May 2011) e1002061.

[53] B. Pieske, M. Sütterlin, S. Schmidt-Schweda, K. Minami, M. Meyer, M. Olschewski, C. Holubarsch, H. Just, G. Hasenfuss, Diminished post-rest potentiation of contractile force in human dilated cardiomyopathy. Functional evidence for alterations in intracellular Ca^{2+} handling, J. Clin. Investig. 98 (3) (August 1996) 764–776.

[54] N. Piroddi, A. Belus, B. Scellini, C. Tesi, G. Giunti, E. Cerbai, A. Mugelli, C. Poggesi, Tension generation and relaxation in single myofibrils from human atrial and ventricular myocardium, Pflügers Archiv - Eur. J. Phycol. 454 (1) (April 2007) 63–73.

[55] M.V. Razumova, A.E. Bukatina, K.B. Campbell, Stiffness-distortion sarcomere model for muscle simulation, J. Appl. Physiol. 87 (5) (November 1999) 1861–1876.

[56] J.J. Rice, F. Wang, D.M. Bers, P.P. De Tombe, Approximate model of cooperative activation and crossbridge cycling in cardiac muscle using ordinary differential equations, Biom. J. 95 (5) (2008) 2368–2390.

[57] J.J. Rice, Y. Tu, C. Poggesi, P.P. De Tombe, Spatially-compressed cardiac myofilament models generate hysteresis that is not found in real muscle, Pac. Symp. Biocomput. (2008) 366–377. PMID: 18229700.

[58] M. Sermesant, F. Billet, R. Chabiniok, T. Mansi, P. Chinchapatnam, P. Moireau, J.-M. Peyrat, K. Rhode, M. Ginks, P. Lambiase, S. Arridge, H. Delingette, M. Sorine, C. Rinaldi, D. Chapelle, R. Razavi, N. Ayache, Personalised electromechanical model of the heart for the prediction of the acute effects of cardiac resynchronisation therapy, 5528. 2009, 239–248.

[59] F. Sheikh, K. Ouyang, S.G. Campbell, R.C. Lyon, J. Chuang, D. Fitzsimons, J. Tangney, C.G. Hidalgo, C.S. Chung, H. Cheng, N.D. Dalton, Y. Gu, H. Kasahara, M. Ghassemian, J.H. Omens, K.L. Peterson, H.L. Granzier, R.L. Moss, A.D. McCulloch, J. Chen, Mouse and computational models link Mlc2v dephosphorylation to altered myosin kinetics in early cardiac disease, J. Clin. Invest. 122 (4) (April 2012) 1209–1221.

[60] R.J. Solaro, Sarcomere control mechanisms and the dynamics of the cardiac cycle, J. Biomed. Biotechnol. 2010 (2010) 1–9.

[61] R. Stehle, B. Iorga, Kinetics of cardiac sarcomeric processes and rate-limiting steps in contraction and relaxation, J. Mol. Cell. Cardiol. 48 (5) (2010) 843–850. PMID: 20060002.

[62] S.G. Tewari, S.M. Bugenhagen, B.M. Palmer, D.A. Beard, Dynamics of cross-bridge cycling, ATP hydrolysis, force generation, and deformation in cardiac muscle, J. Mol. Cell. Cardiol. 96 (July 2016) 11–25.

[63] S.G. Tewari, S.M. Bugenhagen, K.C. Vinnakota, J.J. Rice, P.M.L. Janssen, D.A. Beard, Influence of metabolic dysfunction on cardiac mechanics in decompensated hypertrophy and heart failure, J. Mol. Cell. Cardiol. 94 (May 2016) 162–175.

[64] K. Tøndel, S. Land, S.A. Niederer, N.P. Smith, Quantifying inter-species differences in contractile function through biophysical modelling, Am. J. Phys. 593 (5) (March 2015) 1083–1111.
[65] W. Williams, Huxley's model of muscle contraction with compliance, J. Elast. 105 (1-2) (2011) 365–380.
[66] J. Xi, P. Lamata, J. Lee, P. Moireau, D. Chapelle, N. Smith, Myocardial transversely isotropic material parameter estimation from in-silico measurements based on a reduced-order unscented Kalman filter, J. Mech. Behav. Biomed. Mater. 4 (7) (October 2011) 1090–1102.